a thermal conductivity detector and calibration of nitrogen content was obtained using nitrogen elemental standards.

2.3 Results

Modelled ecosystem (canopy plus ground) fluxes are compared with hourly-averaged eddy covariance flux measurements over the full ten day period in Figure 2.5. Also shown are the ground fluxes as fitted by the inversion procedure. This figure shows that the model was able to successfully predict the diurnal pattern of ecosystem CO_2 fluxes over many days, despite no information on the measured magnitude or overall pattern of the measured fluxes entering the fitting procedure.

The model also predicted reasonable patterns of ecosystem H_2O fluxes, though with some significant departures. Generally speaking, the model partitioned a significant portion of the total evaporation to the soil surface, but the inferred contribution of ground evaporation to the overall evaporation flux varied substantially from day to day (Figure 2.5b). The extreme departures from reasonable values correspond to periods during and following rain, where the model fails to account for wetting of leaf and soil surfaces and subsequent evaporation.

Similarly, the model reasonably predicted both the diurnal pattern and the overall magnitude of sensible heat fluxes (Figure 2.5c). The model found that during the day, the magnitude of the heat flux from the ground was generally much smaller than that from the canopy itself and usually negative in sign. As for the water vapour fluxes, sensible heat fluxes in periods during and following rain were poorly modelled.

The correlation between measured and modelled fluxes as determined by linear regression is shown in Figure 2.6. Data that were deemed to be affected by rain were excluded from the regression analysis, but are shown on the plots. These points were generally the periods up to about three hours after rainfall. This figure shows that there is a degree of scatter for CO_2, H_2O and sensible heat fluxes about the 1:1 line which likely reflects both the inability of the model to perfectly represent all environmental conditions, as well

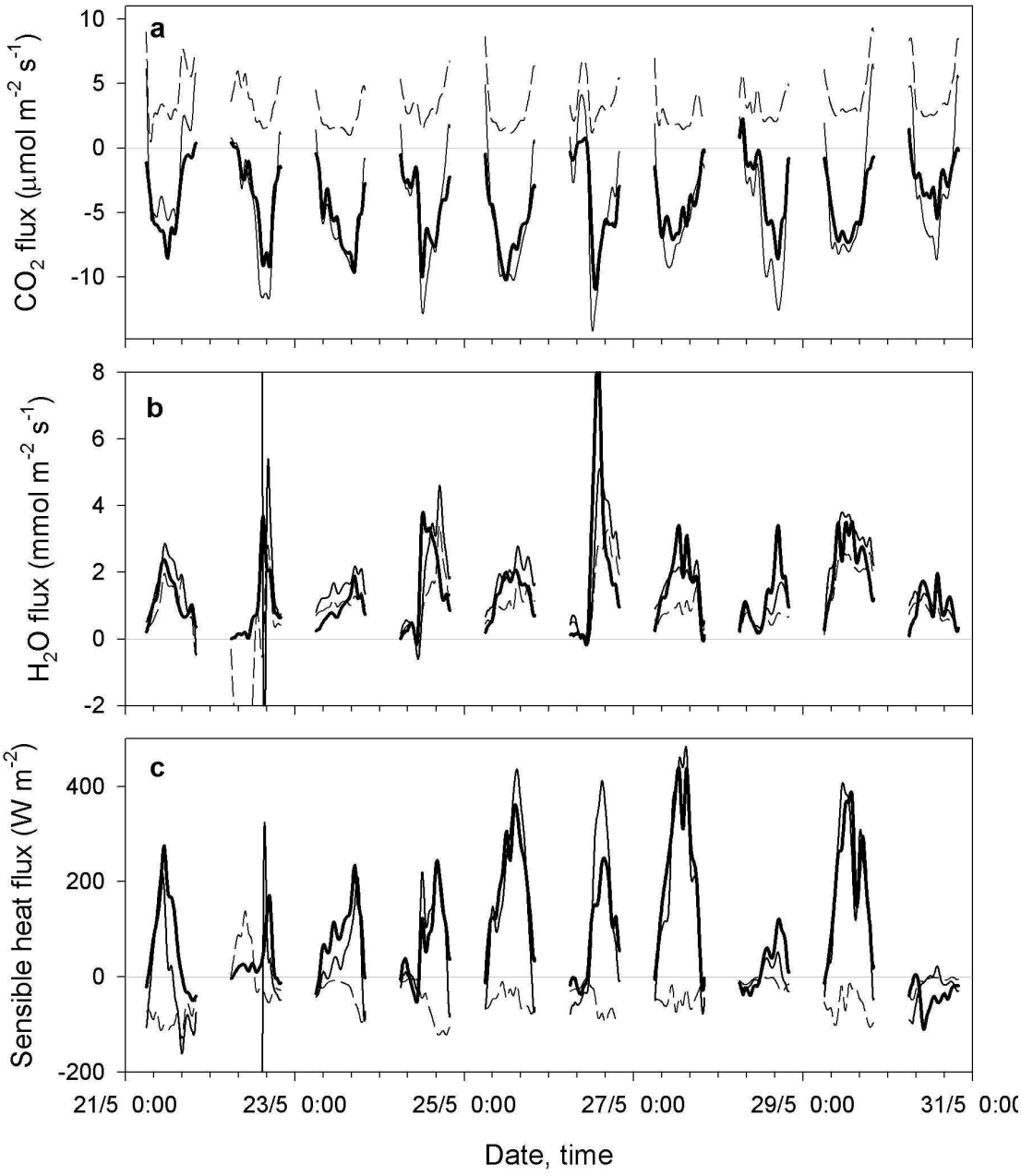

Figure 2.5: Modelled ground flux (dashed line), modelled total flux (thin solid line) and measured total flux (thick solid line) of (a) carbon dioxide, (b) water vapour and (c) sensible heat for daytime hours from 21 to 30 May, 2000.

as random error in the eddy covariance measurements. Correlation was especially low for H_2O fluxes. The regressions show that the model over-estimated H_2O and sensible heat fluxes by about 10%. As this is comparable to the confidence level in the eddy covariance measurements, this disagreement is not serious. The model systematically overestimated CO_2 soil respiratory fluxes when assimilation was low, making the data in Figure 2.6a overshoot the origin. Though not as evident in the figure due to the scaling, this effect was also present for H_2O and heat. This issue relates to thermal stability in the canopy and will be addressed in §2.4.1.

The fit of modelled to measured concentration profiles for the five periods containing isotopic data on each of 25 May and 27 May are shown in Figures 2.7 to 2.11. The model was generally very successful at reproducing the structure of the concentration profiles.

Modelled $\delta^{13}C$ deviates greatly from measurements in the bottom half of the canopy positively in the morning (06:00) on 25 May and negatively in the evening (18:00) on both days. This is a result of incorporation of the storage term in Equation (2.8), which is evidently greatly underestimated for $^{13}CO_2$ compared to $^{12}CO_2$ (recall that $\delta^{13}C$ is a measure of their ratio). Figure 2.11 shows that the same situation applies to $C^{18}O^{16}O$. It was difficult to obtain accurate estimates of storage of $^{13}CO_2$ and $C^{18}O^{16}O$ because isotope samples were taken only every three hours: the period during which the rate of change in concentration is appreciable occurs just after sunrise and has passed by the time of the second flask sampling period at 09:00. The mismatch between the minor and major isotope storage estimates evident in Figures 2.10 and 2.11 occurs despite three-hourly data being used for the major isotope when calculating the effect on $\delta^{13}C$. Discrepancy between measured and modelled $\delta^{13}C$ and $\delta^{18}O$ profiles during other periods is largely attributable to minor sampling error such as undetectable leaks in the sampling lines and exchange of oxygen isotopes with water in the system. Such error was minimised by careful attention to swages and joints along the sampling line, frequent replacement of the dessicant, and minimisation of gravity traps along the sampling line (having as near as possible to a direct, downward line from the measurement height to the flask sampler without loops or

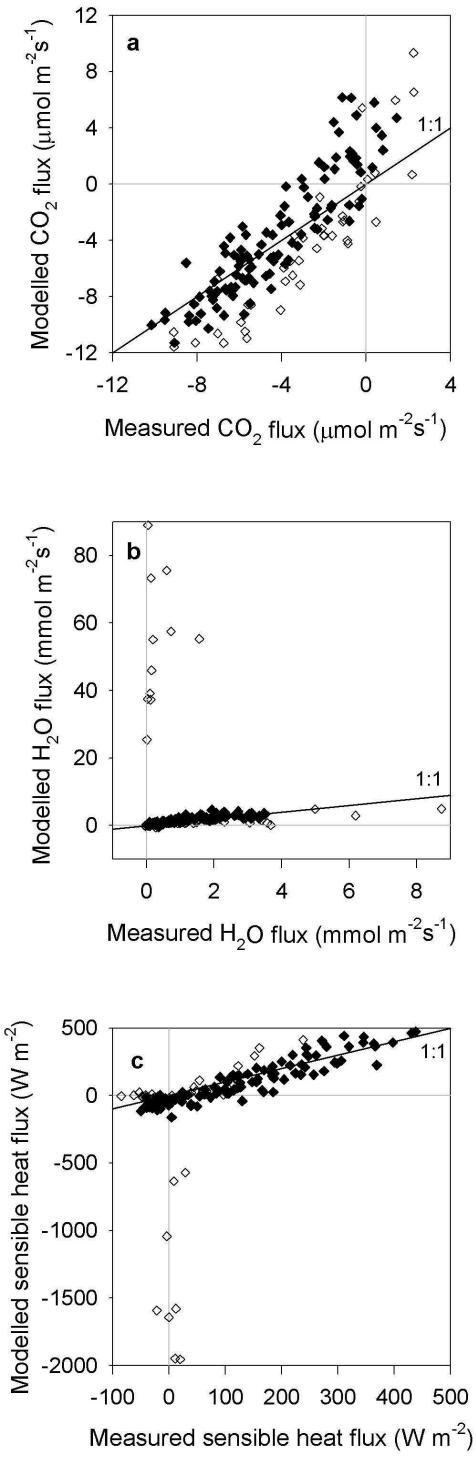

Figure 2.6: Modelled versus measured total (a) carbon dioxide flux, (b) water vapour flux and (c) sensible heat flux for daytime hours from 21 to 30 May, 2000. The 1:1 line is indicated on each graph. Linear regressions fitted through the origin had equations (a) $F_{C,\mathrm{mod}} = 0.99 \pm 0.04 F_{C,\mathrm{meas}}$ ($r^2 = 0.72$), (b) $F_{E,\mathrm{mod}} = 1.12 \pm 0.04 F_{E,\mathrm{meas}}$ ($r^2 = 0.58$) and (c) $F_{H,\mathrm{mod}} = 1.09 \pm 0.04 F_{H,\mathrm{meas}}$ ($r^2 = 0.85$). Open symbols indicate rain-affected points which were excluded from the regression.

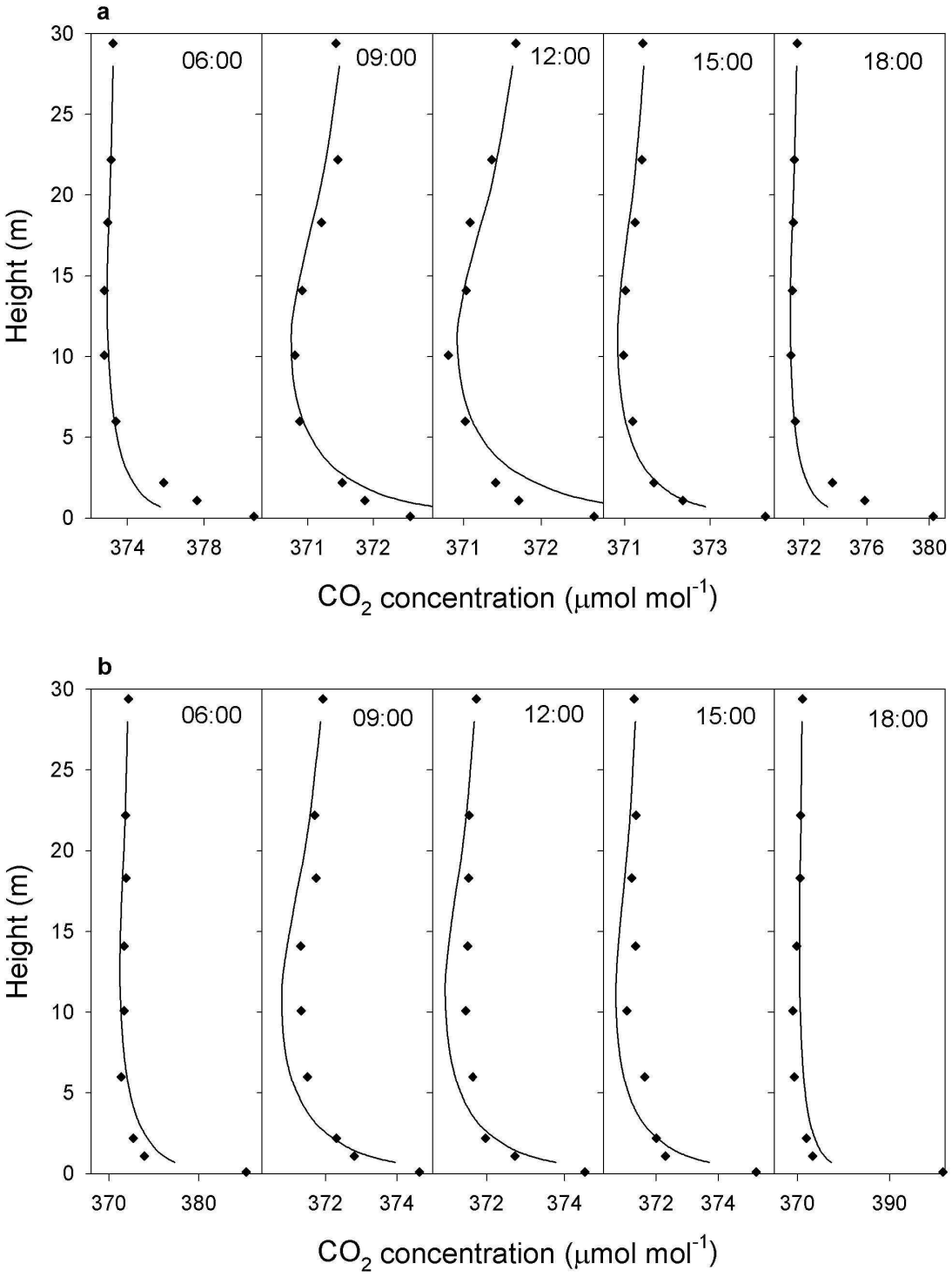

Figure 2.7: Measured (diamonds) and modelled (solid line) CO_2 concentration profiles on (a) 25 May and (b) 27 May, 2000.

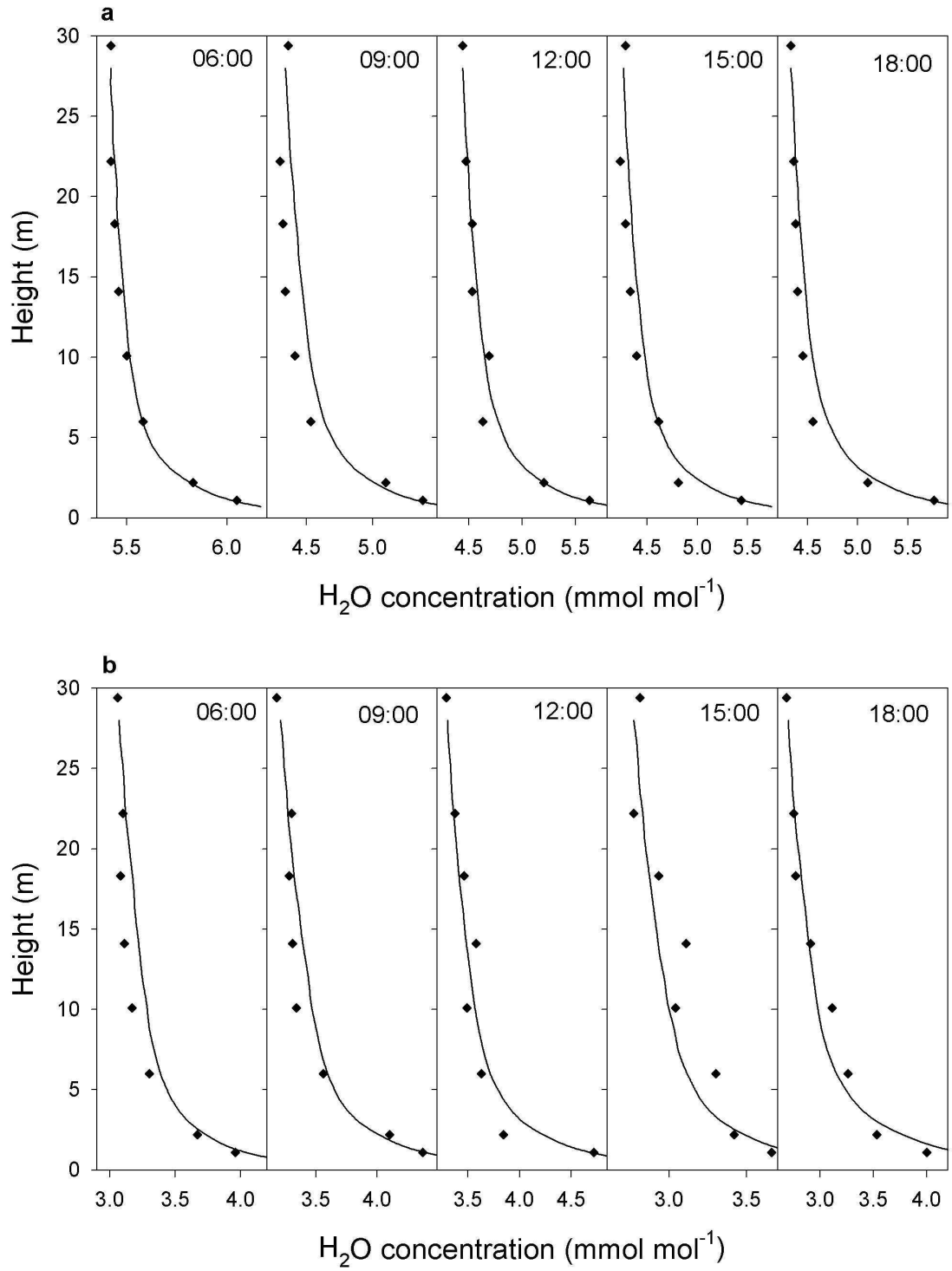

Figure 2.8: Measured (diamonds) and modelled (solid line) H_2O concentration profiles on (a) 25 May and (b) 27 May, 2000.

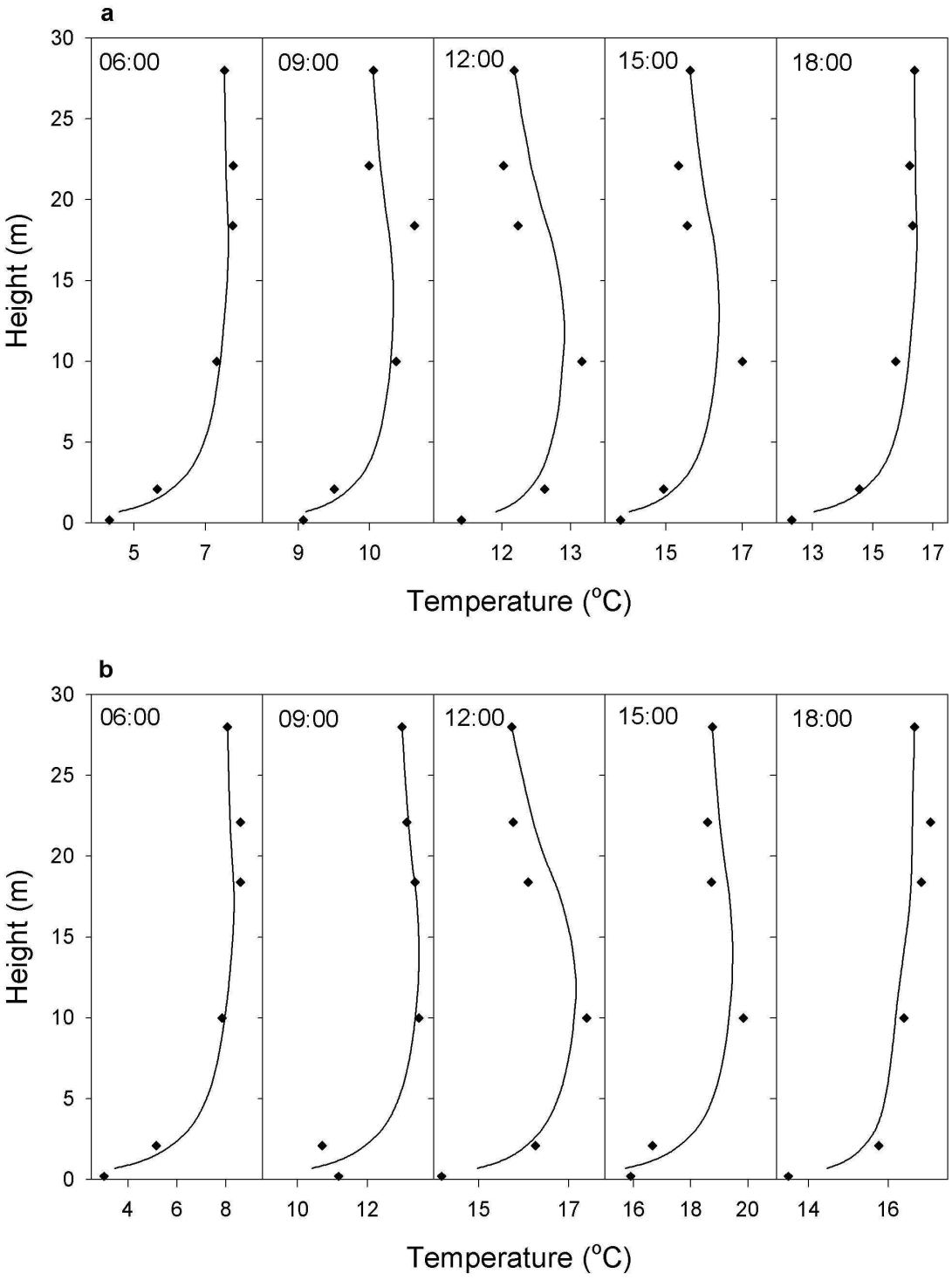

Figure 2.9: Measured (diamonds) and modelled (solid line) temperature profiles on (a) 25 May and (b) 27 May, 2000.

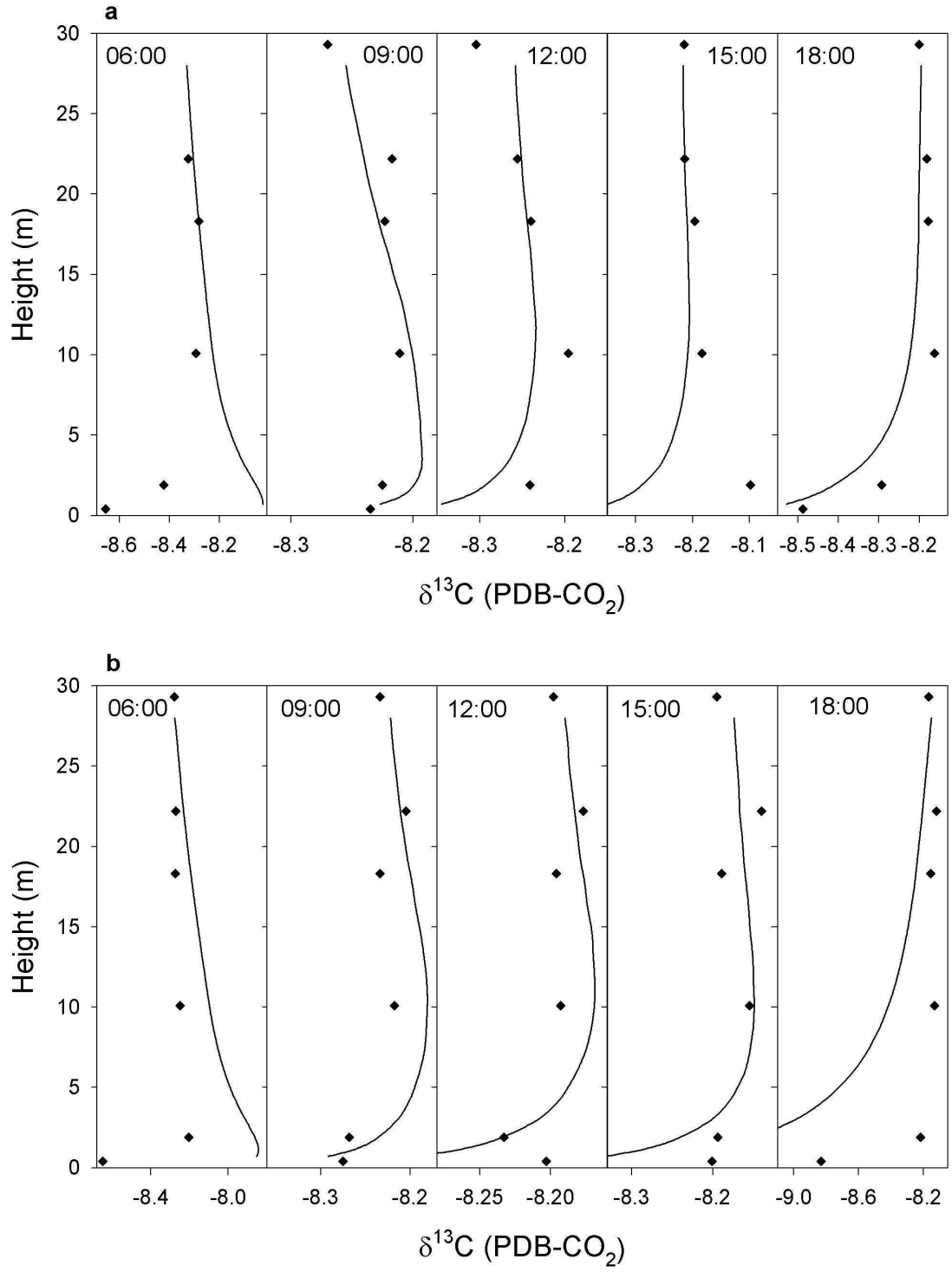

Figure 2.10: Measured (diamonds) and modelled (solid line) δ^{13}C profiles on (a) 25 May and (b) 27 May, 2000.

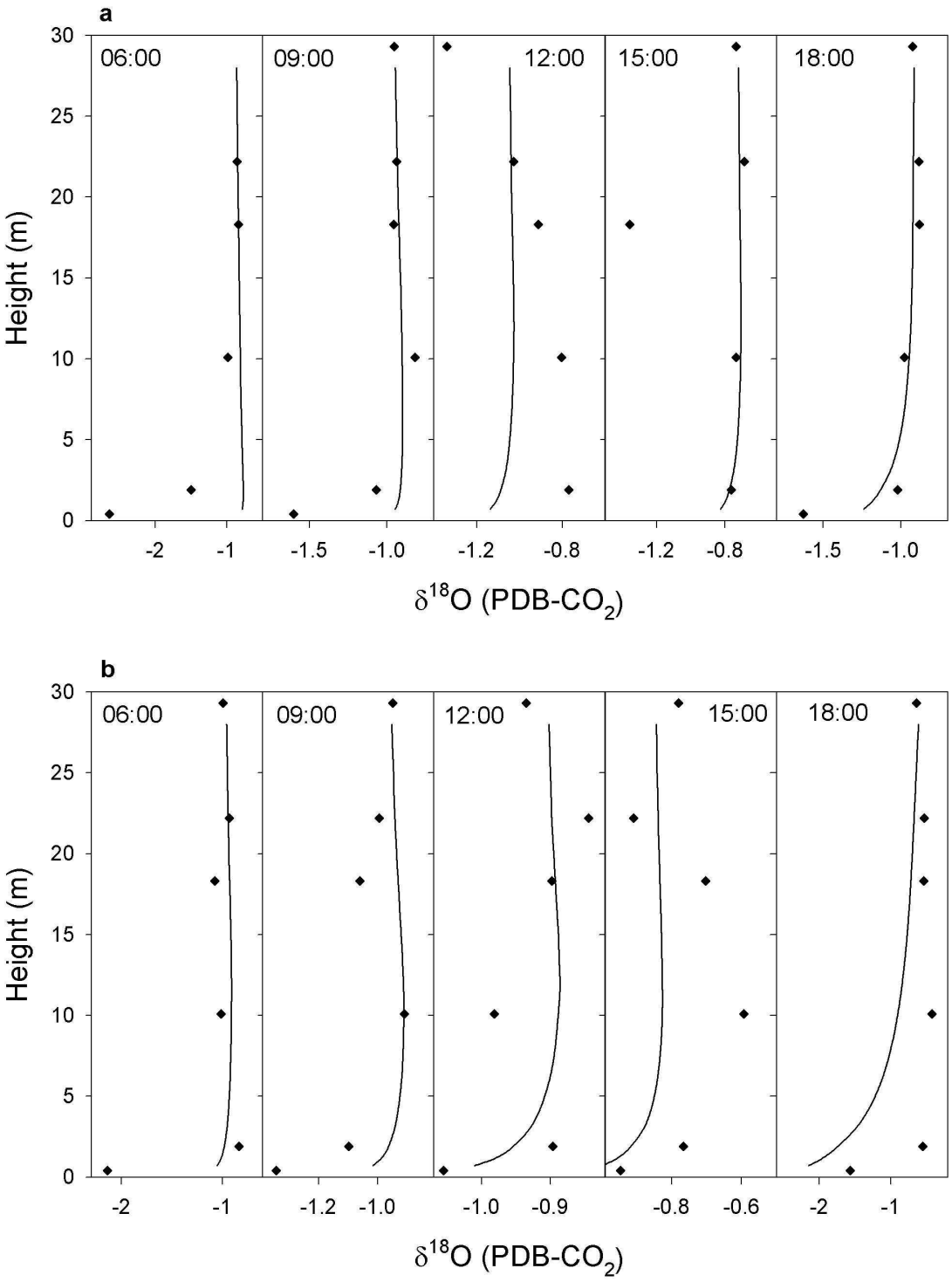

Figure 2.11: Measured (diamonds) and modelled (solid line) δ^{18}O profiles on (a) 25 May and (b) 27 May, 2000.

horizontal stretches where vapour may condense and linger). Measurement error may also explain much of the disagreement in temperature profiles.

Modelled source profiles for CO_2 showed the source peak increasing in magnitude and moving lower in the canopy as solar elevation increased, with the pattern reversing in the evening (Figure 2.12). This is a reflection of the increase in penetration and intensity of radiation during the day. Source profiles for water vapour show a similar pattern (Figure 2.13). Modelled sensible heat source profiles showed that the lower canopy was a slight heat sink in the early morning and evening (Figure 2.14), as the low solar elevation at these times prevented radiation penetrating very deep in the canopy. Source strengths for sensible heat increased in magnitude slowly over the day with the maximum occurring between 12:00 and 15:00.

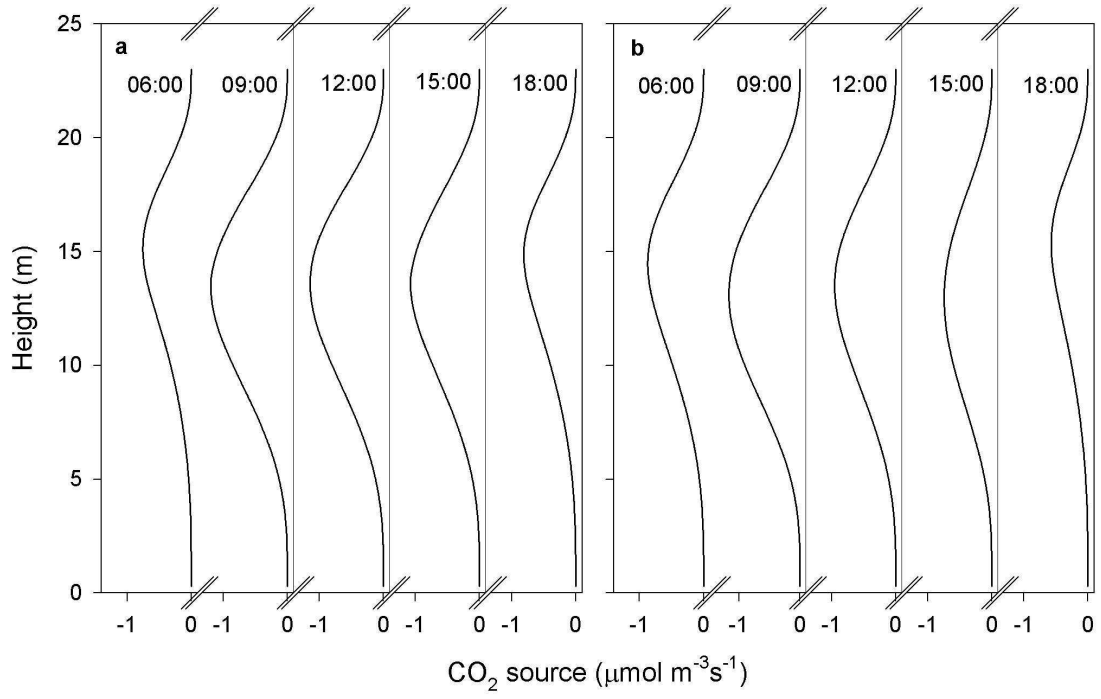

Figure 2.12: Modelled source profiles of carbon dioxide on (a) 25 May and (b) 27 May, 2000.

Micrometeorological properties of the canopy air space including vapour pressure deficit, net radiation and oxygen isotopic composition of water vapour were modelled for the same

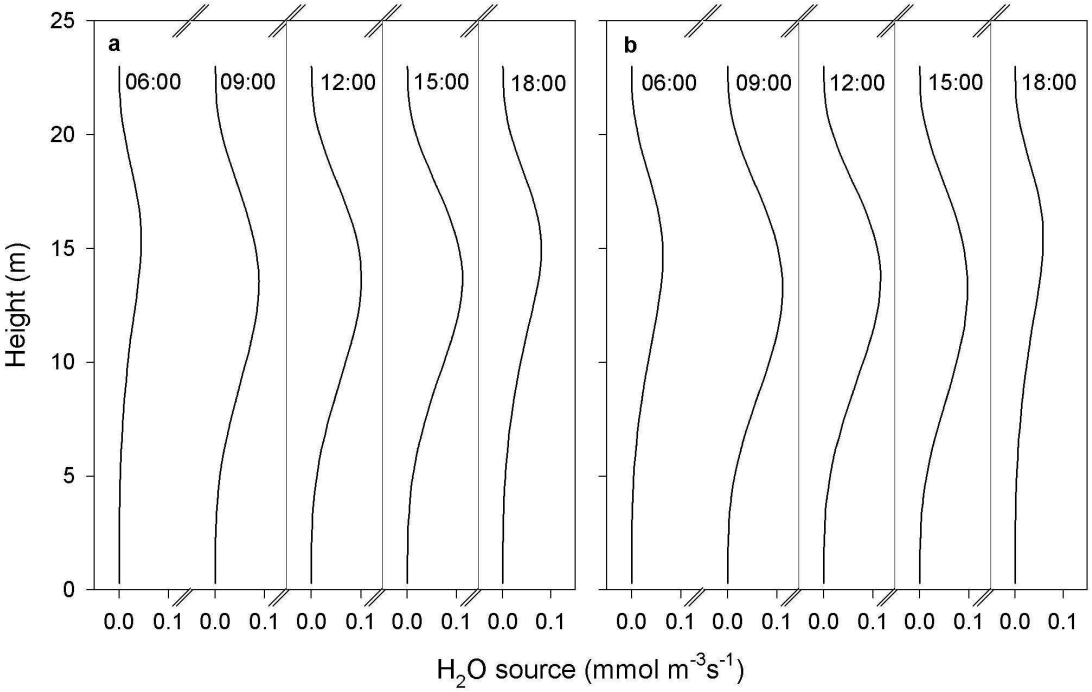

Figure 2.13: Modelled source profiles of water vapour on (a) 25 May and (b) 27 May, 2000.

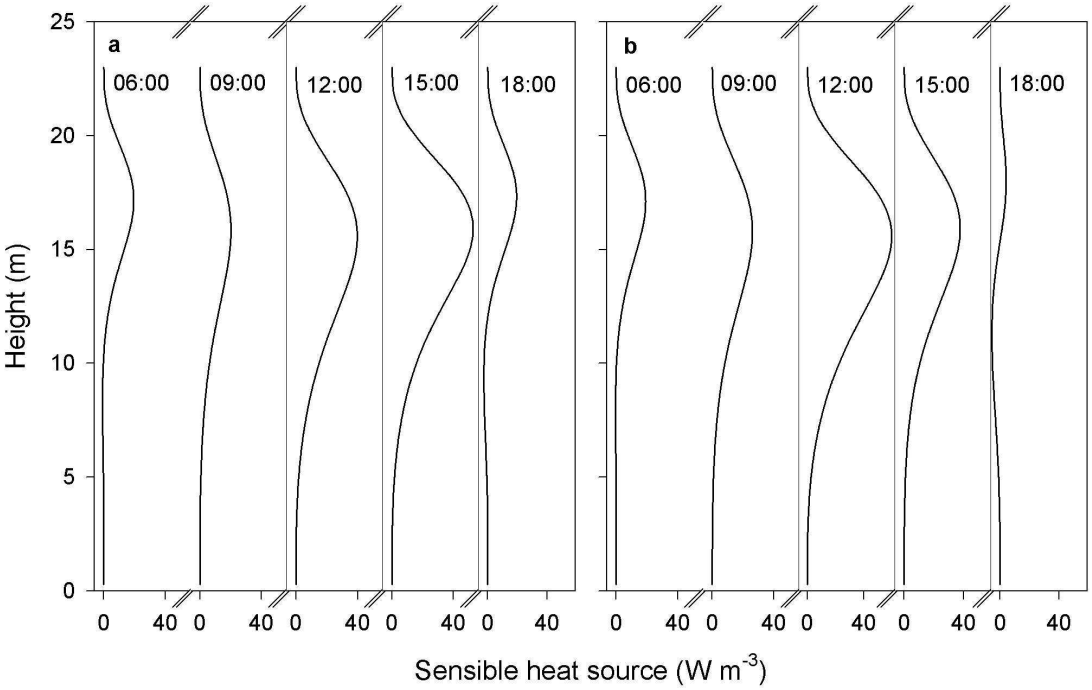

Figure 2.14: Modelled source profiles of sensible heat on (a) 25 May and (b) 27 May, 2000.

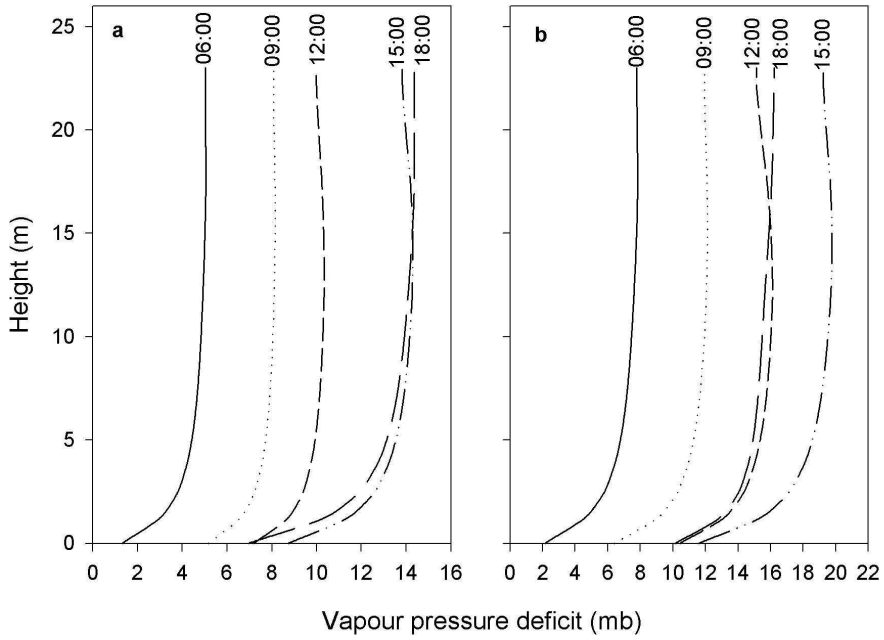

Figure 2.15: Vapour pressure deficit on (a) 25 May and (b) 27 May, 2000, at 06:00 (solid line); 09:00 (dotted line); 12:00 (short dash line); 15:00 (dash-dot-dot line); and 18:00 (long dash line).

periods on 25 and 27 May (Figures 2.15, 2.16 and 2.17). These properties varied vertically and diurnally according to the radiation extinction and leaf energy balance submodels, with isotopic composition of transpired water vapour also being influenced by stomatal conductance.

Most samples for measurement of oxygen isotope composition of water vapour were unfortunately corrupted by evaporation during both collection and transportation, and possibly also during analysis. The few samples for which evaporation was not evident indicated that isotopic composition of water vapour was about two permil enriched compared to the approximate expected value given by composition of source (soil) water (-18‰) minus fractionation during equilibrium evaporation (10.3‰ at 15°C, Majoube, 1971). That is, the measurements were about -26‰ . This two permil difference may indicate evaporation in those samples, evaporative enrichment of soil water near the surface, or conceivably even the addition of enriched vapour from transpiring leaves. Regardless, the measurements were used only to give an approximate value of isotopic composition of water vapour

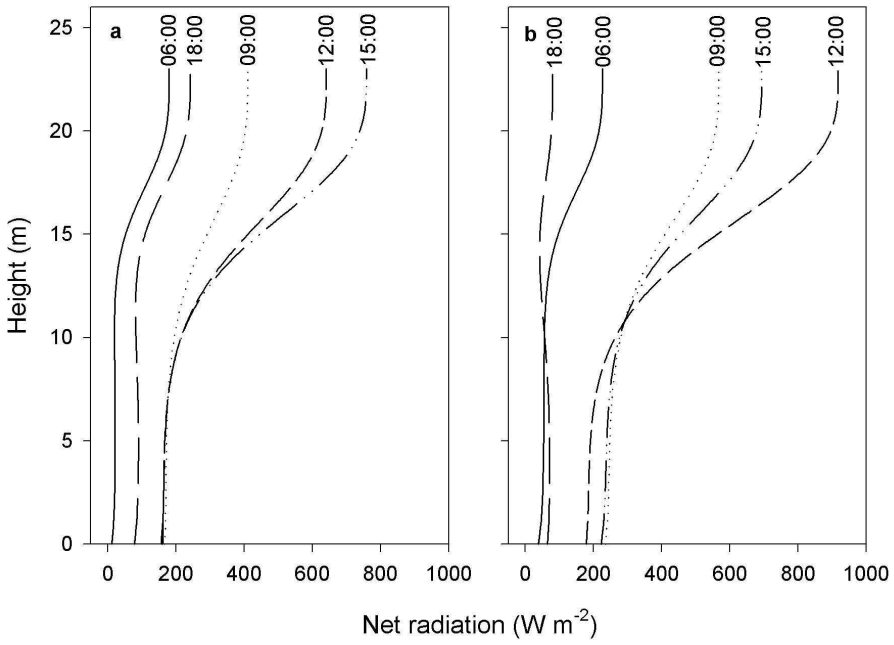

Figure 2.16: Modelled net radiation on (a) 25 May and (b) 27 May, 2000, at 06:00 (solid line); 09:00 (dotted line); 12:00 (short dash line); 15:00 (dash-dot-dot line); and 18:00 (long dash line).

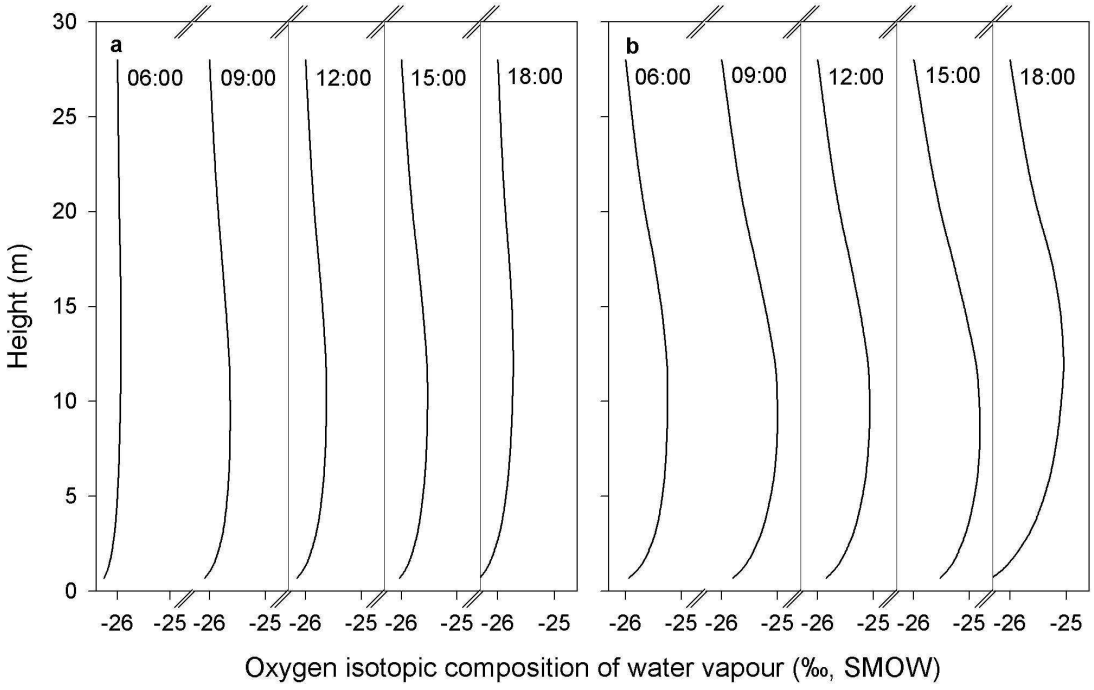

Figure 2.17: Modelled oxygen isotopic composition of water vapour, δ_V on (a) 25 May and (b) 27 May, 2000.

at the top of the canopy, to which modelled variations within the canopy due to transpiration and soil evaporation could be referenced (Figure 2.17). It is interesting to note that the peak in enrichment of water vapour occurs much lower in the canopy than the peak in transpiration rate (compare Figures 2.17 and 2.13). This offset is also apparent in the positioning of peak in temperature profiles compared to the heat source profiles (Figures 2.9 and 2.14), and is probably due to the lower mixing rate in the lower canopy. It is also evident from Figure 2.17 (note all scales are the same) that the much higher vapour pressure deficit on 27 May (Figure 2.15) gave rise to much greater enrichment of water vapour in the canopy air space on that day due to the higher transpiration rate carrying relatively isotopically heavy soil water composition.

The biochemical and physiological constraints in the model allowed physiological properties of the leaves to be predicted, as well as their variation with height. Modelled profiles of stomatal conductance (g_{sc}) reflected the effect of transition from Rubisco-limited to light-limited assimilation rates, causing a sharp decline in stomatal conductance through the canopy in the morning and evening profiles (Figure 2.18). Daytime profiles were additionally influenced by the strong peak in assimilation rate in the middle canopy (see Figure 2.12), causing a slower decrease or slight increase in stomatal conductance through the canopy before the sharper decrease due to light limitation. Conductance was modelled to increase near the ground due to the decrease in vapour pressure deficit there (see Figure 2.15), though the assumed leaf area distribution (Figure 2.1) has leaves starting only at about 2m height, so that the model predictions of physiological properties below that height are unimportant. Diurnal variation in the magnitude of stomatal conductance at the top of the canopy was driven by increasing vapour pressure deficit, giving a negative trend in g_{sc}, as well as by assimilation rate, which maintained relatively high conductances in the middle of the day.

The ratio of intercellular to ambient CO_2 concentration (c_i/c_a) was modelled to be fairly constant with height except for a very slight decrease in the middle canopy corresponding to decreasing stomatal conductance, and then a larger increase near the ground

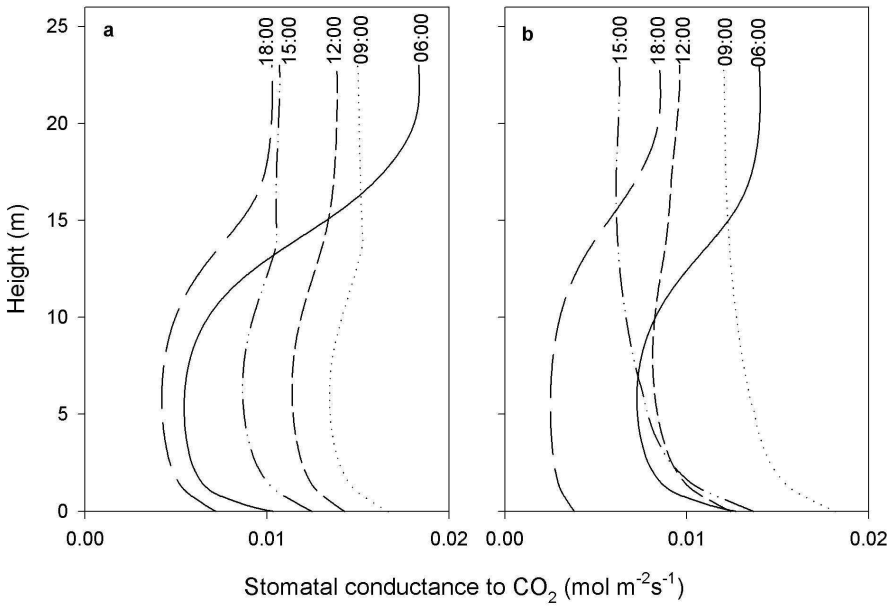

Figure 2.18: Modelled stomatal conductance to CO_2 on (a) 25 May and (b) 27 May, 2000, at 06:00 (solid line); 09:00 (dotted line); 12:00 (short dash line); 15:00 (dash-dot-dot line); and 18:00 (long dash line).

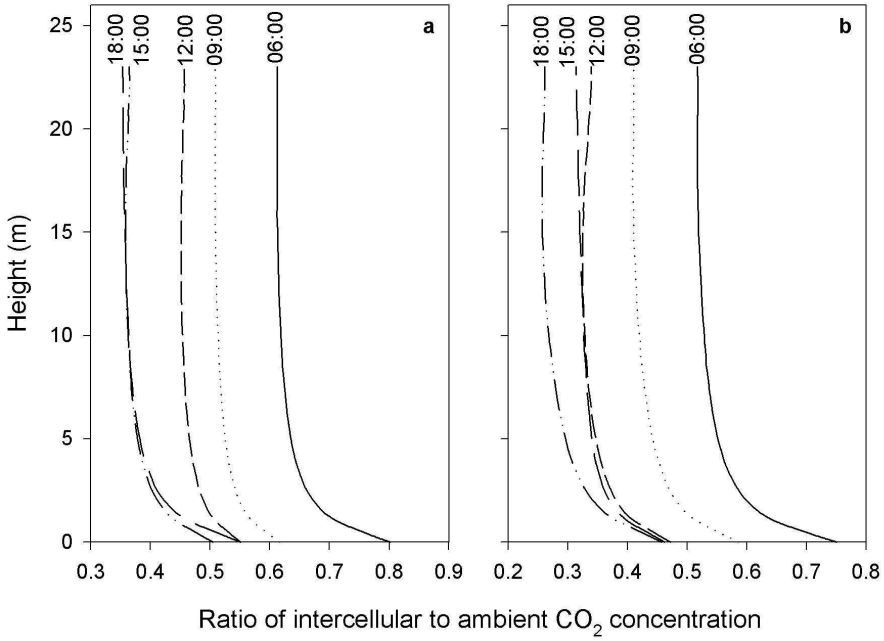

Figure 2.19: Modelled ratio of intercellular to ambient CO_2 concentration (c_i/c_a) on (a) 25 May and (b) 27 May, 2000, at 06:00 (solid line); 09:00 (dotted line); 12:00 (short dash line); 15:00 (dash-dot-dot line); and 18:00 (long dash line).

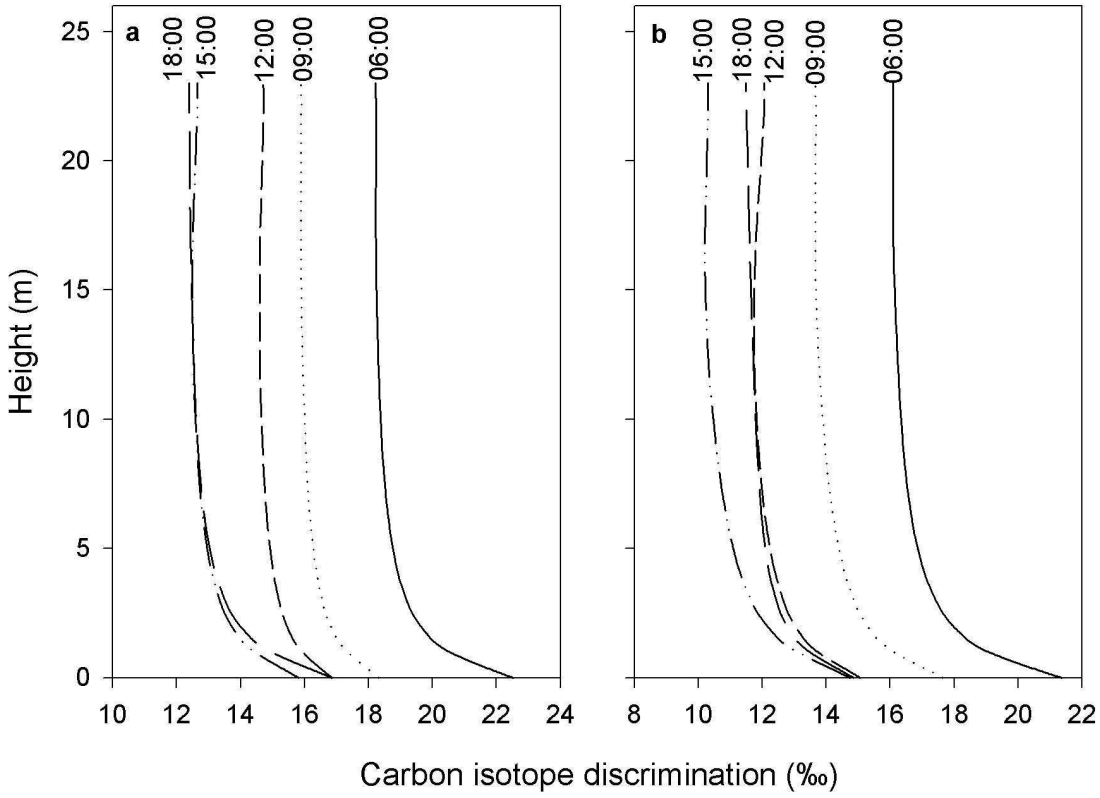

Figure 2.20: Modelled carbon isotope discrimination on (a) 25 May and (b) 27 May, 2000, at 06:00 (solid line); 09:00 (dotted line); 12:00 (short dash line); 15:00 (dash-dot-dot line); and 18:00 (long dash line).

as high water vapour concentrations there encourage stomatal opening (Figure 2.19, refer also to Figure 2.18). c_i/c_a decreases during the day from a high of about 0.6 in the morning of 25 May, becoming steady at about 0.4 by 15:00 (Figure 2.19a). Values on 27 May were even lower, ranging from just over 0.5 in the morning to just under 0.3 in the evening (Figure 2.19b). The significance of these low values is discussed in §2.4.4.

As expected from the simplified relation of Equation (2.21), profiles of carbon isotope discrimination closely followed c_i/c_a (Figure 2.20), with the main feature being an increase of about 4‰ near the ground compared to the top of the canopy. This would have little influence on isotopic composition of ambient CO_2, however, because the leaf area

distribution and light limitation restrict assimilation to the middle and upper canopy (Figure 2.12). The magnitude of discrimination decreased over the day from about 18.5‰ to 12.5‰ on 25 May and from 16.5‰ to 10.5‰ on 27 May.

Oxygen isotope composition of leaf water modelled using Equation (2.23) showed a strong enrichment during the day on both 25 and 27 May due to increasing evaporation as vapour pressure deficit (VPD) increased (Figure 2.21, refer also to Figure 2.15). There was also a decreasing gradient in leaf water composition near the ground which followed the gradient in VPD.

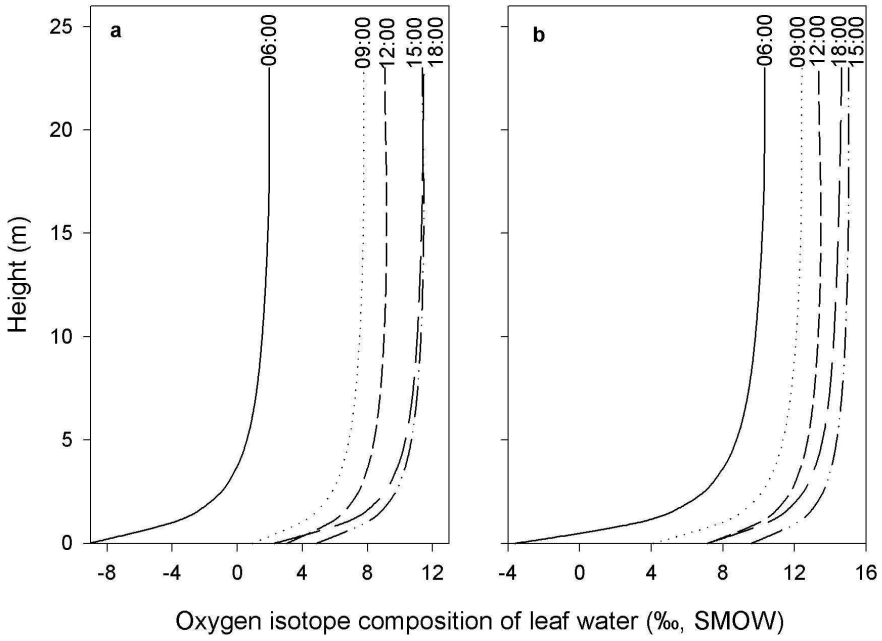

Figure 2.21: Modelled oxygen isotope composition of leaf water on (a) 25 May and (b) 27 May, 2000, at 06:00 (solid line); 09:00 (dotted line); 12:00 (short dash line); 15:00 (dash-dot-dot line); and 18:00 (long dash line).

Oxygen isotope discrimination showed no clear diurnal trend due to the two conflicting influences of vapour pressure deficit (Figure 2.22). Firstly, increasing VPD drives an increase in evaporative enrichment of leaf water isotopic composition, which would lead to a positive trend in ^{18}O discrimination through exchange of oxygen isotopes with CO_2 in the chloroplast (Equations (2.22) and (2.23)). Secondly, increasing VPD also causes

a decrease in stomatal conductance and hence c_i/c_a (and hence c_c/c_a) during the day, driving a negative trend in ^{18}O discrimination (Equation (2.22)). The net result of these influences is that there is no particular diurnal pattern in oxygen isotope discrimination, with the order in profiles from morning to evening varying between the two days (Figure 2.22).

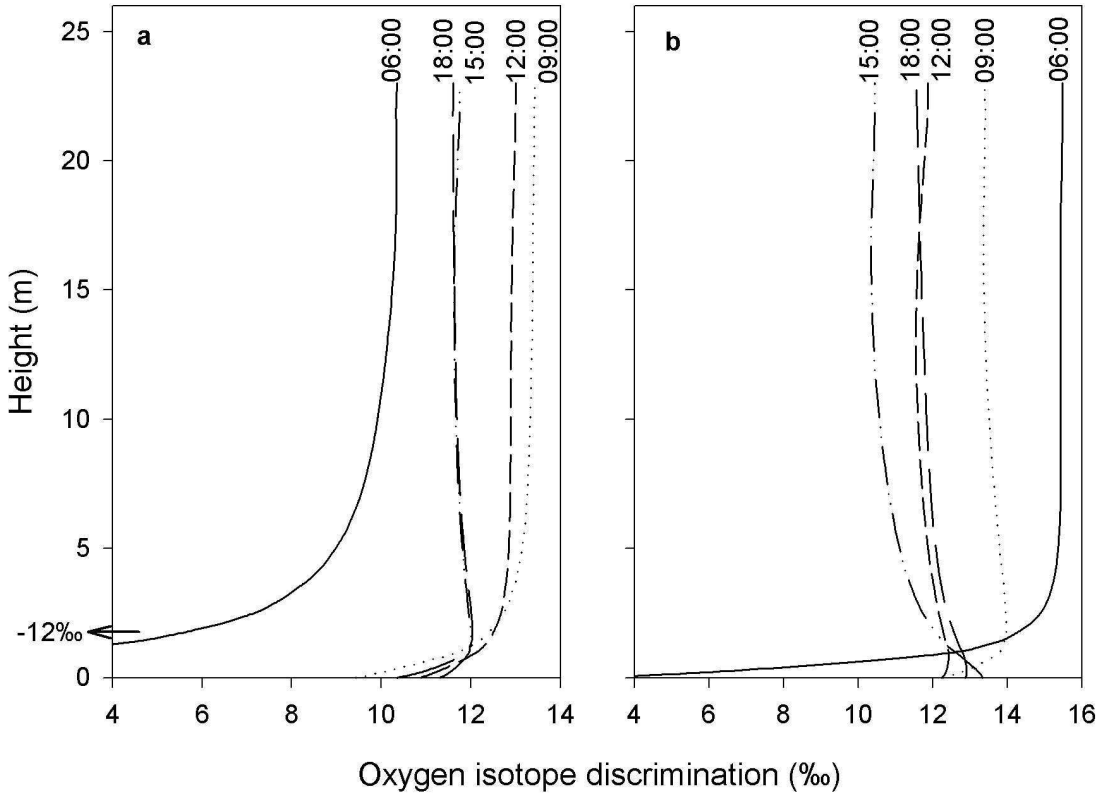

Figure 2.22: Modelled oxygen isotope discrimination on (a) 25 May and (b) 27 May, 2000, at 06:00 (solid line); 09:00 (dotted line); 12:00 (short dash line); 15:00 (dash-dot-dot line); and 18:00 (long dash line).

2.4 Discussion

2.4.1 Stability effects

Modelled flux magnitudes were consistently overestimated in the early morning and late evening. This is a common finding in similar modelling studies and most likely results

from stable stratification in the lower canopy. In a thermally stratified layer displaced air parcels have a tendency to return to their former position. Turbulent eddies are therefore dampened and the Lagrangian time scale T_L may be significantly reduced. Gravity waves may propagate, causing an increase in σ_w without contributing to scalar transport. Stability effects are expected to be particularly important for tall canopies where strong temperature inversions may exist at the ground. Further complications may result from the variation of density of roughness elements (leaves and stems) with height, allowing stability to vary with height.

A correction for stable stratification may be applied based on Monin-Obukhov surface layer similarity functions, modified for the canopy layer only in the definition of the stability parameter as the ratio of canopy height to Obukhov length, $\zeta = h/L_O$ (Shaw *et al.*, 1988; Leclerc *et al.*, 1990; Leuning, 2000). The Obukhov length in the surface layer is given by $L_O = u_*^3\bar{\theta}/\left[\kappa g\left(\overline{w'\theta'}\right)_0\right]$, where $\bar{\theta}$ is the mean potential temperature; κ is the von Karman constant; g is the acceleration due to gravity; and $\left(\overline{w'\theta'}\right)_0$ is the heat flux at the surface. Standard surface layer similarity functions (see for example Kaimal and Finnigan, 1994) may then be used to correct for effects on σ_w and T_L.

To apply the stability correction in this manner the Obukhov length must be known or estimated. To demonstrate the effect of this correction L_O was arbitrarily chosen to give stability ranging from highly stable ($\zeta = 0.5$) for the hourly periods beginning at 06:00, 19:00 and 20:00, moderately stable ($\zeta = 0.2$) for 07:00 and 18:00, slightly stable ($\zeta = 0.05$) for 08:00, 09:00 and 17:00, and neutral otherwise. Comparison of measured and modelled total fluxes for the ten day period with stability correction is shown in Figure 2.23. This shows a considerably improvement for all fluxes, though still with a degree of scatter especially in the H_2O fluxes and a tendency for underestimation of sensible heat fluxes at the lower end. The modelled total H_2O fluxes were strongly driven by modelled ground fluxes because canopy transpiration was often modelled to be rather small except on 25 and 27 May, the only two days unaffected by cloud or rain. Regression of modelled versus measured fluxes with stability correction applied were practically 1:1 for H_2O and

heat fluxes, while CO_2 fluxes were overestimated by about 13% compared to the eddy covariance measurements. As stated above, this level of disagreement is not significantly different from the expected accuracy of the eddy covariance measurements.

Other measures of stability exist which are more appropriate to application within tall plant canopies where considerable variation in stability with height may exist. For example the Brunt-Vaisala frequency given by $N = \left(\frac{g}{T_0}\frac{\partial\bar{\theta}}{\partial z}\right)^{0.5}$ is the frequency of oscillation of a displaced particle in a stably stratified flow. Then the typical displacement distance can be estimated as σ_w/N. This is a local measure of stability that can be used to give a stability profile within the canopy. Another local stability measure is given by the Richardson number, $Ri = \frac{g}{\bar{\theta}}\frac{\partial\bar{\theta}/\partial z}{(\partial u/\partial z)^2}$, which has been related to the Obukhov length in the surface layer (Kaimal and Finnigan, 1994). Investigation of these stability measures and the adjustment of Lagrangian time scale and σ_w from them remains for further work, with the present stability correction serving merely to demonstrate the potential to account for model divergence in the early morning and late evening. The stability issue is discussed further in relation to T_L in §2.4.4, p.80.

2.4.2 Surface energy budget

Of relevance to the comparison of modelled sensible and latent heat fluxes with the eddy covariance measurements is the degree of closure obtained in the energy budget for the measurements. Commonly, eddy covariance measurements attain in the order of 80-90% closure for a variety of reasons including differing footprints of the flux and radiation sensors, losses due to horizontal divergence and low frequency losses due to insufficient averaging time (Lee, 1998; Finnigan and Leuning, 2000; Finnigan *et al.*, 2002). In this study daily sensible and latent heat flux accounted for 85% of available energy, with losses thought to be partly attributable to spatial heterogeneity of canopy reflectance (trees versus gaps), partly to horizontal divergence, but perhaps mostly due to the half hour averaging period used. In terms of available energy, the model is driven by radiation measurements above the canopy, so a combined (positive) discrepancy between modelled

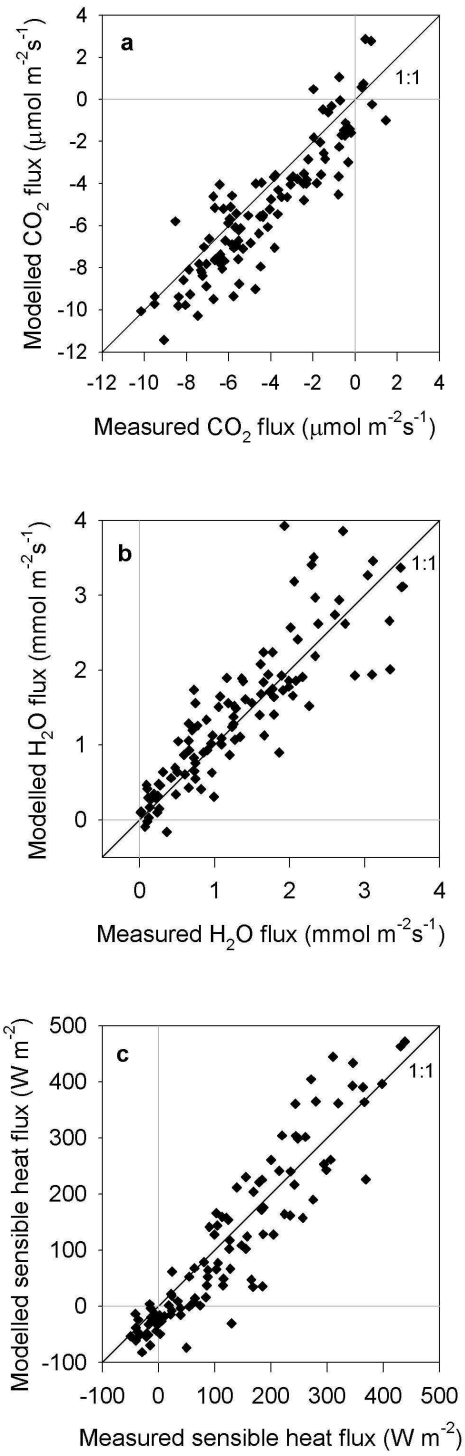

Figure 2.23: Modelled versus measured total (a) carbon dioxide flux, (b) water vapour flux and (c) sensible heat flux, with stability correction applied, for daytime hours from 21 to 30 May, 2000. The 1:1 line is indicated on each graph. Linear regressions fitted through the origin had equations (a) $F_{C,\mathrm{mod}} = 1.13 \pm 0.03 F_{C,\mathrm{meas}}$ ($r^2 = 0.78$), (b) $F_{E,\mathrm{mod}} = 1.02 \pm 0.03 F_{E,\mathrm{meas}}$ ($r^2 = 0.75$) and (c) $F_{H,\mathrm{mod}} = 1.00 \pm 0.03 F_{H,\mathrm{meas}}$ ($r^2 = 0.84$). Rain-affected points are not shown.

and measured sensible and latent heat fluxes of up to about 18% can be explained by the energy imbalance in the measurements. Figure 2.6 shows that the model did indeed overestimate sensible and latent heat fluxes by about 10% compared to the eddy covariance measurements, but Figure 2.23 shows that this can be fully accounted for by stability effects. Since the stability correction applied here was somewhat crude, it is possible that the closure problem may partially contribute to the overestimation present in the uncorrected data.

2.4.3 Determination of ground fluxes

One test for the validity of the inferred ground evaporation rates comes from the observations of Kelliher *et al.* (1997) and Kelliher *et al.* (1998). Working in larch and pine stands in Siberia, respectively, they observed that rates of understorey evaporation were always close to the equilibrium evaporation rate under moist conditions (see also Schulze *et al.*, 1999). It seems reasonable to assume that a similar relationship should hold for the ground evaporation rate in the current study. Equilibrium evaporation was therefore calculated as $\lambda_E E = \frac{\varepsilon}{1+\varepsilon}(R_{n,g} - G)$, where $\varepsilon = \frac{s\lambda_E}{c_p}$; $R_{n,g}$ is the net radiation at the ground; and G is the soil heat flux, estimated as 10% of $R_{n,g}$. The slope of saturation vapour pressure with temperature s was calculated at temperature averaged through the canopy space (Raupach, 2001a discusses the significance of temperature in the evaluation of equilibrium evaporation). Modelled soil evaporation was about half the equilibrium evaporation rate on 25th and 27th May. On other days, when there was generally significant cloud and/or rain, there was no correlation between modelled and equilibrium soil evaporation. Combining the equilibrium soil evaporation rate with modelled canopy transpiration gave total water vapour flux in good agreement with eddy covariance measurements, suggesting that the deficiency in the model lay in the determination of soil evaporation rather than canopy transpiration.

One reason why the model was less successful in determining soil evaporation is that the sign of the ground flux is the same as the canopy flux for water vapour. For heat

and CO_2 the canopy flux opposes the ground flux, producing a strong enrichment and depletion, respectively, in temperature and CO_2 concentration in the mid-canopy layer, while the water vapour concentration generally decreases monotonically with height. This is the likely reason why correlation between modelled and measured H_2O fluxes was much poorer than for CO_2 and heat, though the situation was greatly improved with the stability correction (Figure 2.23).

Better determination of ground fluxes may be obtained if closer attention is paid to concentrations near the ground. Initial optimisations using modelled concentrations from about 1.5m height upwards gave very poor estimates of ground fluxes, particularly for water vapour. In the analysis presented here interpolated concentrations were used at 20 evenly spaced heights from 0.5m to the reference height at 28m, with non-negligible weight given only to those heights closest to the measurement heights. The lowest measurement heights for each species ranged from 0.1m to 0.4m, so that the minimum height of 0.5m used in the model may not have fully represented the strong gradients measured near the ground. This may have biased the model towards better optimisation of canopy fluxes than ground fluxes, even though in general the below-canopy region was spatially better-sampled than within the canopy (see §2.2.2). This lower limit in the modelled concentrations was applied to avoid potential problems both with heterogeneity in concentrations so close to the ground, requiring extra spatial sampling, and with characterisation of the turbulence regime in this region, for which there is little observational base.

2.4.4 Determination of parameters

Limitations of the optimisation method

The optimisation procedure outlined in Appendix D uses a gradient-descent method to find the local minimum and hence may not successfully discover the global minimum. Additionally, the goodness of fit function may be slowly varying with respect to the parameters (that is, have a flat minimum), so that similarly adequate fits to the data may be obtained with significantly different parameter values. An alternative optimisation method that overcomes some of these difficulties is the "genetic algorithm". This method

assesses the performance of randomly generated parameter values, keeping track of those "traits" or parameter combinations which give best results, until an optimal set is found. The advantage of the genetic algorithm method is that because the optimisation picks parameter values at random, it is not led into a local minimum as can happen with the gradient-descent method. The disadvantage is the vastly greater number of iterations required to find the minimum. In addition, the gradient-descent method generates as a matter of course the covariance matrix of the standard errors in the fitted parameters (see Appendix D), while the genetic algorithm requires additional simulations for parameter confidence estimates. In the present study the model was run on a desktop computer and computational resources were therefore quite limited. These reasons and time limitations meant that the genetic algorithm method was not investigated here.

Parameter covariances and error estimates

It was found that the model could not sufficiently distinguish between parameter influences to always be effective in determining optimum independent values. For example considering the water vapour profile, an increase in flux at the ground will cause an increase in concentration near the ground, while an increase in T_L will mix this contribution higher in the canopy. Furthermore, an increase in λ leads to an increase in stomatal conductance and hence canopy transpiration, but the effect of this on concentration within the canopy also depends on the magnitude of T_L. Hence changes in ground flux and λ can be almost entirely offset by changes in the T_L profile. Maximum photosynthetic capacity and λ are also correlated, with a reduction in either leading to lower stomatal conductance and lower assimilation and transpiration rates.

Ideally there would be enough information available in the structure of the concentration profiles for each species to tease out the relative influences of covarying parameters. More information may potentially be gleaned by altering the relative weight given to concentration data of each species, if the precision of the data permits. Initial analysis based

on estimated instrument precision showed that the CO_2 concentration data were the major driving force because the instrument precision relative to the absolute measurement was by far the best for CO_2. It was found that this favouritism could be slightly reduced without unduly testing the precision limit of other species, and giving more weight to the water vapour and temperature profiles allowed better characterisation of hydrologic and energetic exchange processes.

The relative weight given to each scalar species significantly influenced the optimised parameter values. As stated above, assigning weight according to measurement precision caused the CO_2 measurements to overwhelm all other species in the optimisation. Investigation of the cost function χ^2 (see Appendix D) associated with each species reflected this bias, with that for CO_2 being by far the greatest. The weight given to each species was therefore adjusted to be spread more evenly, by choosing "errors" associated with each species that produced cost functions as close as possible to that for CO_2. The cost function for H_2O remained quite low, however, because of the very small variation in H_2O concentration with height. Attempts to further decrease the error associated with the H_2O measurements in order to increase its cost function resulted in numerical instability in the program. The absolute scale of the errors (standard deviations in the measurements) was chosen so that in general the deviation of modelled concentration from measured concentration at each measurement height was about one standard deviation.

Correlation coefficients were calculated for each pair of parameters (Appendix D) as a measure of the degree of covariance between parameters. High negative correlation ($\sim$-0.7) was found between λ and V_l, presumably due to their similar effect on stomatal conductance which could be compensated for by an opposite increment in the other parameter. This meant that the while some combination of the two parameters such as the sum or product was well constrained, the individual parameters were not. While of concern to the robustness of the optimisation, some confidence in the optimised values for these two parameters could be assumed because they were both significantly less than the prior estimates, implying that no compensating positive and negative trends were occurring.

In initial runs when less weight was given to the temperature profiles in the optimisation, the diffuse and direct radiation extinction coefficients k_d and k_b were highly correlated ($\sim$+0.7). This is of more concern because the correlation is positive and optimal values for both parameters deviated in the same direction from the prior estimates. Unfortunately the ratio between these two parameters could not be guessed at with any confidence because of the highly complicated influences expected from leaf scattering, clumping and particularly penumbra, which redistributes the intensity of non-intercepted light. This correlation decreased, however, when more weight was given to the temperature profiles, and was insignificant for the optimisation presented.

Finally, the two parameters defining the Lagrangian time scale were negatively correlated ($\sim$-0.8), indicating that the vertical structure in concentration profiles was insufficient to characterise the shape of the Lagrangian time scale within the canopy. The parameter a_1 defining the rate of decline of T_L within the canopy was therefore set at a relatively high value (30, at which point the two parameters are uncorrelated because a very large change in a_1 is then required to give a significant change in the average canopy T_L), and the remaining parameters re-optimised. This had very little effect on the optimal values found for the other parameters, indicating that the assumption of constant T_L in the canopy except very close to the ground (setting $a_1 = 30$) may be a better option in the present model. An alternative option, allowing T_L to vary with time to account for varying stability, is explored below (p.80).

Confidence intervals for the optimal parameter values were calculated from the error covariance matrix (Appendix D), assuming that the measurement errors were normally distributed. These confidence intervals are representative of both the error in values obtained in the optimisation due to covariance of parameters and level of sensitivity of modelled concentrations to each of the parameters, as well as the error in the model formulation - that is, the ability of the model to accurately portray a real canopy. The magnitude of the error estimates obtained depends on the standard error assigned to the concentration measurements. Shown in the first column of Table 2.4 are the error estimates and confidence

intervals for parameters when the modelled concentrations differ from the measurements by about one standard deviation (1σ) on average. The increase in assigned measurement error applied in order to achieve agreement within 1σ accounts for the inability of the model to perfectly reproduce reality. The errors here therefore give an indication of the combined uncertainty in parameter values due to both the model formulation and the optimisation. In the second column are the errors and confidence intervals obtained when the measurements are given their *a priori* error estimates according to instrument precision. Note that the latter errors correspond to different optimised parameter values. These errors represent the error in the optimisation alone. The values shown in Table 2.4 indicate that the error in the optimisation is generally very low, while that due to the model formulation is much larger. The errors assigned to the measurements to obtain model agreement within 1σ ranged from one to about ten times those estimated from instrument precision, with temperature being the least divergent and CO_2 the most.

Parameter	Value, $c_{mod} - c_{meas} \sim \sigma_c$	Standard error (95% confidence intervals), $c_{mod} - c_{meas} \sim \sigma_c$	Value, *a priori* σ_c	Standard error (95% confidence intervals), *a priori* σ_c
λ	130	20 (90-170)	135	2 (131-139)
V_l	32	4 (18-34)	26.9	0.5 (25.9-27.9)
k_b	0.37	0.05 (0.27-0.47)	0.41	0.02 (0.37-0.45)
k_d	0.20	0.05 (0.10-0.30)	0.44	0.05 (0.34-0.54)
a_1	23	5 (13-33)	13.9	0.2 (13.5-14.3)
a_2	0.25	0.02 (0.21-0.29)	0.301	0.002 (0.297-0.305)

Table 2.4: Parameter error estimates and confidence intervals

As the final result of interest is the leaf-level and canopy fluxes rather than the parameters themselves, it is worth investigating the propagation of errors in the parameter estimates to the calculated fluxes. For V_l and λ this is straightforward, as Equations (2.4), (2.5), (2.10) and (2.16) show that the leaf-level flux of CO_2 is proportional to V_l when Rubisco-limited, or $2.1V_l$ when light-limited, and leaf-level fluxes of CO_2 and H_2O are proportional to $\sqrt{\lambda}$. The order of the effect on canopy fluxes will then be in proportion

to V_l and $\sqrt{\lambda}$. With the standard error estimated for the parameters when modelled concentrations differed from measurements by about 1σ (Table 2.4, column 2), the error in fluxes of CO_2 and H_2O from that in λ is about 40%, while error in CO_2 fluxes from that in V_l is 15%. Investigation of the effect of error in the radiation extinction coefficients and Lagrangian time scale indicated an influence of around 20% on fluxes of heat, CO_2 and H_2O. These large error estimates are somewhat misleading, however, because the modelled fluxes rely on a non-linear combination of all these parameters and an alteration in one will be compensated for by adjustment of the others to maintain model agreement with concentration measurements. The combination of parameters specified in the model that lead to the flux estimates is therefore likely to be better-constrained than the individual parameters themselves, leading to less error in flux estimates than suggested above.

Optimised parameter values

Marginal water loss per unit carbon gain

The optimised value found for λ of 130 mol mol^{-1} is significantly lower than the values estimated by Lloyd *et al.* (2002b), Arneth *et al.* (2002a) and Lloyd and Farquhar (1994) for this biome. A larger value, however, greatly increased the modelled canopy transpiration to levels irreconcilable with eddy covariance measurements. An independent estimate of this parameter may be obtained using the eddy covariance measurements and simple estimates of ground fluxes: a plot of daily eddy covariance measurement of water vapour flux minus calculated equilibrium soil evaporation against measured daily CO_2 flux minus an assumed constant soil respiration rate of 1.5 μmol m^{-2}s^{-1} gave a slope of 60 mol mol^{-1} (r^2=0.6). While the ratio of marginal water loss to marginal carbon gain would in general be expected to be greater than the ratio of transpiration to assimilation, the difference becomes small at low conductances.

These low estimates for λ indicate considerable hydraulic limitation. The cause of this limitation seems likely to be low temperature, particularly the near-freezing soil temperatures. Low soil water content may be discounted as a contributor because the ground

was constantly wet from snow-melt. The difference between the estimates found here and those found by Arneth *et al.* and Lloyd and Farquhar's review may be explained by seasonal variation, with the latter estimates being obtained in the summer period, or response of different species. The data of Lloyd *et al.* suggest little seasonal variation, but a comparison of their study site (Scots pine, Zotino west) with the present one (Siberian fir and spruce, Zotino east) for the 2000 season showed that the east side, with greater nutrient availability, tended to achieve higher assimilation rates earlier in the season, while in summer assimilation and transpiration rates were roughly equal at the two sites. Being subject to the same hydraulic limitation would then give the east side a lower marginal water loss per unit carbon gain. Other experimental evidence has shown that on a time scale of several days, different coniferous species respond differently to emergence from winter. Photosynthetic recovery from cold inhibition in red spruce occurred before increases in stomatal conductance (Schaberg *et al.*, 1995), while transpiration increased quickly in Scots pine after removal from winter conditions, followed by a much slower recovery of photosynthetic rate (Zelawski and Kucharska, 1967).

There is some theoretical and experimental evidence in the literature to suggest that low temperature may reduce λ. A model investigation of water use efficiency (CO_2 assimilated per unit of water transpired, WUE) in a lodgepole pine forest predicted that as temperature decreased from 35 to 5°C under constant relative humidity, WUE would increase from 1.5 to 6 mmol mol^{-1} (Nikolov *et al.*, 1995), corresponding to a decrease in λ from 670 to 170 mol mol^{-1} (calculated here as the inverse of WUE). A similar temperature response was found under constant vapour pressure deficit. Interestingly, the same model applied to aspen predicted no decrease with temperature. The difference resulted from different parameter values estimated from field measurements for the two species in the stomatal conductance model (in their case the Ball *et al.* (1986) model), with aspen generally having higher stomatal conductance and lower water use efficiency. Hydraulic limitation has been linked to stomatal closure (Ryan and Yoder, 1997), and in the spring snow-melt the low temperatures may have significant effects on plant hydraulics through

increased viscosity of water and decreased root permeability, thereby causing a reduction in stomatal conductance (Ishida *et al.*, 2001). In addition, intercellular CO_2 concentration has been found to decrease with decreasing temperature, inferred both from measurements in a single canopy on different days (Price and Black, 1990) and from the trend in $\delta^{13}C$ with latitude for a range of species (Körner *et al.*, 1991). Carbon isotope discrimination has also been found to decrease with increasing hydraulic limitation (Panek, 1996), implying decreasing intercellular CO_2 concentration, though Cernusak and Marshall (2001) found this effect to be relatively small and suggested changes in leaf area and leaf morphology were more important. The balance of evidence suggests, however, that relatively high assimilation rates may be maintained at low temperatures while transpiration is reduced.

Maximum photosynthetic capacity

The optimised value found for photosynthetic capacity of 26 μmol $m^{-2}s^{-1}$ was also significantly lower than the prior estimate, but still within the range found for coniferous species reported by Wullschleger (1993). The low value found here may well reflect post-winter recovery as discussed by Bergh *et al.* (1998). Inhibition of photosynthesis due to freezing soil and air temperatures has been widely observed in coniferous species over periods from hours to days (eg. DeLucia, 1986; Öquist and Ögren, 1985; Ottander and Öquist, 1991). Additional experimental evidence suggests a longer term adjustment to climate conditions as, for example, needles become frost-hardened and chlorophyll content declines over winter, and new chlorophyll is synthesised in spring (Vogg *et al.*, 1998; Lloyd *et al.*, 2002b; Öquist and Huner, 2002).

Photosynthesis in a *Pinus sylvestris* forest near the present study site was observed to recover to relatively high rates within a week of snow-melt (Arneth *et al.*, 2002b), while also exhibiting a slower response through the growing season with maximum rates not achieved until late in the season, lagging the maximum in photosynthetically active radiation (Lloyd *et al.*, 2002b). These two stages of recovery may reflect the various short and long term cold response mechanisms touched upon above (see Lloyd *et al.*, 2002b for

discussion). The low value for maximum photosynthetic capacity (and hence maximum electron transport rate) found here is consistent with these arguments.

Radiation extinction coefficients

The prior estimates for radiation extinction coefficients represented the theoretical values for leaves of random distribution and orientation intercepting a point source of radiation (which for diffuse light was integrated over the whole sky). As these conditions do not reflect reality very closely, it is not surprising that the optimised values were considerably different to the prior estimates. The direction of change is as one would expect from effects such as leaf clumping and penumbra. The former effect would allow greater penetration of both diffuse and direct light, while the latter would similarly increase penetration but at the expense of intensity. Modelled net radiation below the canopy was 30% more than that measured by the two net radiometers at 2m height, as determined by regression through the origin for hourly averaged data from 21 May to 30 May (slope = 1.3, $r^2 = 0.4$, see Figure 2.24). Rain-affected periods and periods in the afternoon when the radiometers were in direct sunlight were excluded from the regression. The poor correlation found with measured data was most likely due to insufficient spatial averaging by the two radiometers. Some systematic error in the model may have been present, however, as the relationship between modelled and measured net radiation at the ground was not linear, being steeper at the low end and flattening at high radiation (Figure 2.24). Net radiation at the ground modelled using the prior estimates for k_b and k_d was unreasonably small.

Attempts to model radiation penetration accounting for leaf clumping, canopy gaps and penumbra in coniferous canopies have generally not been verified in the field due to difficulty in obtaining the required measurements (Lemeur and Blad, 1974; Palmroth *et al.*, 1999). Ross *et al.*, 1998 (further developed in Ross and Mõttus, 2000a, 2000b) tested their statistical model of radiation penetration in a willow coppice plantation with reasonable success but found that error and incomplete spatial representation in the measurements were limiting, and suggested that generalised application to canopies in the field, if found

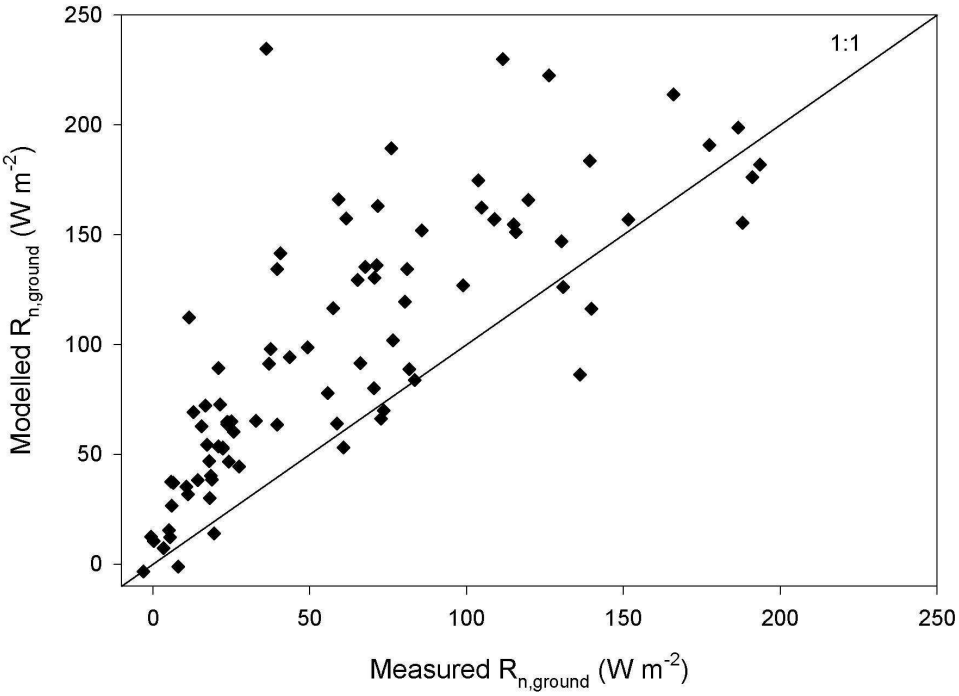

Figure 2.24: Modelled versus measured net radiation at the ground for daytime hours from 21 to 30 May, 2000. Linear regression fitted through the origin had equation $R_{n,mod} = 1.3R_{n,meas}$, $r^2 = 0.4$

appropriate, would require further characterisation of empirical coefficients. Many studies at the shoot level have shown that shoot structure and its variation within the canopy plays an important role in distribution of light interception, leaf area density, and canopy photosynthesis, particularly when the diffuse radiation fraction is low (Oker-Blom, 1986; Leverenz and Hinckley, 1990; Wang and Jarvis, 1993; Stenberg, 1996a; Stenberg, 1998; Stenberg *et al.*, 1998; Palmroth *et al.*, 1999).

In addition to its influence on canopy photosynthesis, radiation interception is also used to infer leaf area index (LAI). Considerations of needle clumping, tree gaps and penumbra have been applied to optical methods for deducing LAI in a manner similar to the radiation penetration models mentioned above, in order to reconcile these methods with direct leaf area measurements (Gower and Norman, 1991; Chason *et al.*, 1991; Stenberg, 1996b; van Gardingen *et al.*, 1999).

Finally, needle clumping affects the spectral reflectance properties of coniferous canopies. Studies have shown that reflectance in the PAR and NIR regions decreases significantly as the scale of investigation increases from needle to shoot to canopy (Williams, 1991; Rock *et al.*, 1994). This has implications for modelling radiative transfer within canopies, as well as for remote sensing.

The general lesson to be learnt from the studies mentioned in this section is that needle clumping, tree gaps and penumbral effects are very important when considering radiation interception in coniferous canopies. To account for these effects in a detailed and rigorous manner is perhaps for the present impractical in the field because of the great detail and quantity of measurements of canopy and shoot structure required. The approach taken in the present study, while forcing the diffuse and direct radiation components to follow an exponential decline within the canopy, does allow the rate of extinction to be optimised to find the photosynthesis, transpiration and heat exchange profiles that give the best fit to the measured concentration profiles. Allowing the direct and diffuse components to vary simultaneously gave rise to potentially high correlation between the extinction coefficients depending on the relative weight given to the concentration species, but could perhaps better account for the slightly different effects of needle clumping and penumbra than would a fixed ratio between the two.

Lagrangian time scale

Determination of the parameters defining the Lagrangian time scale was hindered by stability effects in the lower canopy which were not constant in time. This meant that the model had to simultaneously optimise for daytime neutral or slightly stable conditions and for very stable conditions in the early morning and late evening when the ratio of T_L to h/u^* should be lower than in neutral conditions. The optimised scaling factor a_2 was lower than the prior estimate of 0.3, most likely partially accounting for the stable conditions.

One approach to overcome this difficulty is to allow T_L to be optimised for each profile set individually, varying over the day and even between days as stability changes. The problem then is whether enough information is realistically available to achieve a reasonable evolution of T_L profiles with stability. Alternatively, if the stability correction described above (§2.4.1) is considered adequate, the optimisation could take place with stability correction "on". Investigation of the latter approach showed that a much higher value for the T_L scaling factor a_2 was found when optimised with stability correction applied. This was to such an extent that the model became unable to effectively reproduce concentration profiles during the day, indicating the dominant influence of the morning and evening profiles on the optimisation of T_L. Investigation of the former approach, optimising for time-varying T_L, showed that the optimised scaling factor a_2 had a tendency for lower values in the morning and evening on 25 May (Figure 2.25a). There was also considerable variation in the rate of decline in the canopy defined by the factor a_1, which similarly tended to produce relatively lower T_L in the lower canopy in the morning and evening on 25 May. The optimisation on 27 May (Figure 2.25b) accorded less with expectations from stability influences, perhaps due to this being a much calmer day so that the contrast between conditions in the morning or evening compared to the day was less pronounced.

2.4.5 Isotopic discrimination and plant physiological characteristics

Carbon isotope discrimination was modelled to vary considerably over a day, with the value at midday, roughly corresponding to the time of maximum assimilation rate, being about 15‰ on 25 May and 12‰ on 27 May (Figure 2.20). This is much lower than has been previously estimated for boreal forest in both modelling and experimental investigations (18-19‰ , eg. Lloyd and Farquhar, 1994; Flanagan *et al.*, 1996; Fung *et al.*, 1997; Buchmann *et al.*, 1998). The low values for Δ^{13}C found here correspond to low modelled intercellular CO_2 concentrations (Figure 2.19) and are consistent with the low stomatal conductance (Figure 2.18) arising from the optimised marginal water loss per unit carbon

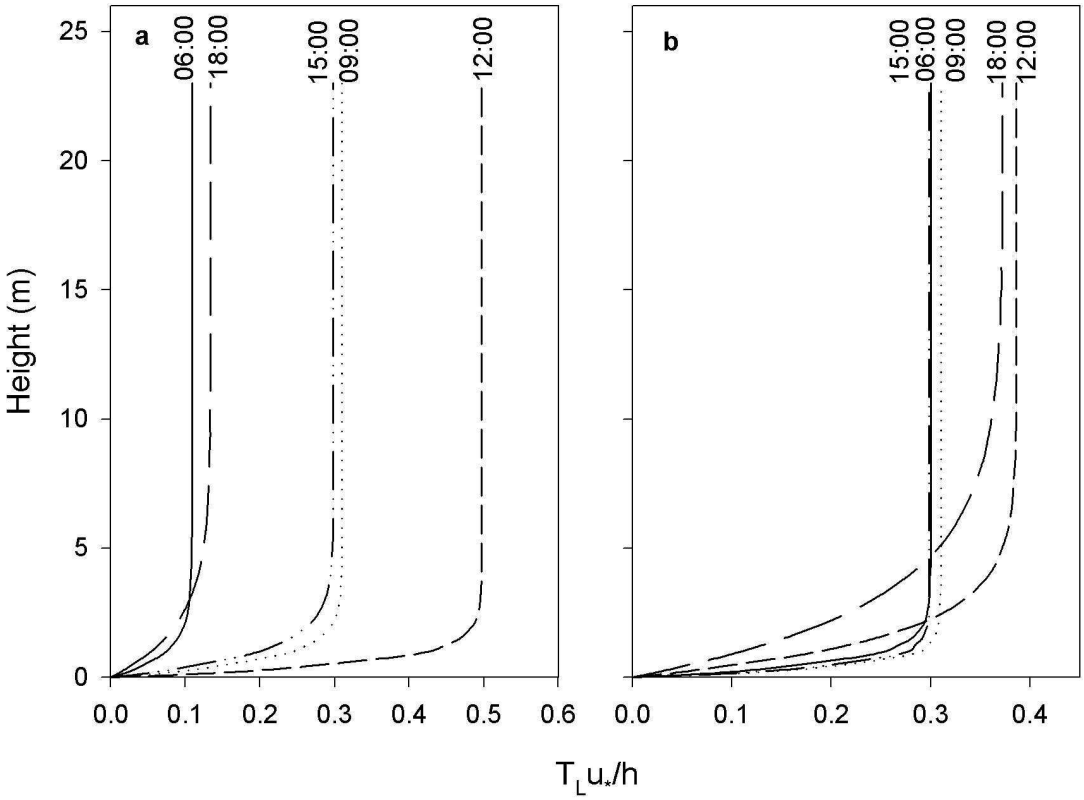

Figure 2.25: Modelled ratio of Lagrangian time scale T_L with h/u_* on (a) 25 May and (b) 27 May, 2000, at 06:00 (solid line); 09:00 (dotted line); 12:00 (short dash line); 15:00 (dash-dot-dot line); and 18:00 (long dash line).

gain. As discussed above, this may be a seasonal effect as the plants experience hydraulic limitation and possibly also depressed photosynthetic capacity during emergence from the very cold winter. The lower discrimination inferred on 27 May compared to 25 May, along with lower modelled stomatal conductance and c_i, are a result of that day being much warmer and drier (Figures 2.9 and 2.8).

Modelled oxygen isotope discrimination was generally around 12-14‰ , comparable to previous estimates and measurements in boreal forests (∼10‰ , Farquhar *et al.*, 1993; ∼20‰ , Flanagan *et al.*, 1997). Several other global modelling studies, however, estimate much lower oxygen isotope discrimination in central Siberia, due to their low estimates for oxygen isotope composition of leaf water (-3‰ , Ciais *et al.*, 1997; ∼0‰ , Cuntz *et*

al., 2002). These low leaf water compositions (compare Figure 2.21) arise from use of much higher humidity in those models than was observed at the present study site (∼80% compared to 20-40% here). Conditions in mid-summer at this site would be expected to lead to further divergence from those models as source water would become enriched following the seasonal trend in precipitation.

Profiles of isotope discrimination and plant physiological properties presented here are in line with expectations in some cases, and somewhat surprising in others. The very low values found for stomatal conductance, intercellular CO_2 concentration and carbon isotope composition rely strongly on the accuracy of a single optimised parameter, λ. Further investigation of this parameter over a larger data set including seasonal variation needs to be carried out before the value found here can be fully accepted. Additionally, the optimisation of this parameter is dependent on the formulation of exchange processes within the model, and is particularly influenced by the specification of radiation penetration. The various submodels used here can only approximately represent the complex canopy system, and over-simplifications within the model formulation may at times bias the model towards unrealistic parameter solutions by way of compensation. Indeed, the optimisation of radiation extinction coefficients was intended to compensate for omission of known complications to radiation penetration. Nevertheless, the concentration data obtained in the present study could not be reproduced within the model using prior estimates of parameters, indicating that additional information was obtained by the optimisation procedure. The results shown here can therefore be viewed with a degree of confidence.